Proceedings of the Institution of Civil Engineers
Geotechnical Engineering 159
January 2006 Issue GE1
Pages 49–59

Paper 13980

Received 24/09/2004
Accepted 27/04/2005

Keywords:
Dams/embankments/geotechnical engineering

Abbas Soroush
Head of Civil and Environmental Engineering Department, Amirkabir University of Technology (Tehran Polytechnic), Iran

Ata Aghaei Araei
Senior Geotechnical Engineer, Building and Housing Research Centre (BHRC), Tehran, Iran

ice

Analysis of behaviour of a high rockfill dam

A. Soroush and A. Aghaei Araei

This paper reviews the effects of first impounding on rockfill dams. In particular, saturation collapse phenomena induced by wetting of rockfills are highlighted. Major attention is given to the effects of impounding-induced saturation on the mechanical behaviour of rockfills. The paper presents a comprehensive study of the behaviour of the Masjed-E-Soleyman rockfill dam during its construction and first impounding, by means of thorough analyses of instrumentation results and numerical modelling. Results of the instruments show that impounding-induced saturation collapse has occurred in the upstream shell of the dam. Also, the numerical analyses suggest that the Hardening Soil, elasto-plastic constitutive model employed in the analysis, using reduced strength and stiffness parameters for the saturated rockfills, is able to capture the behaviour of the rockfill dam during the first impounding. The results of the analysis compare well with the similar results of the instrument monitoring.

NOTATION

c	cohesion
CH	chainage
E_{50}^{ref}	secant stiffness in standard drained triaxial test
$E_{\text{oed}}^{\text{ref}}$	tangent stiffness for primary oedometer loading
$E_{\text{ur}}^{\text{ref}}$	stiffness in unloading and reloading
El.	elevation
h	overburden height
k_{h}	horizontal permeability
k_{v}	vertical permeability
MC	moisture content
m	exponent factor for stress-level dependence of stiffness
PI	plasticity index
P_{ref}	reference stress for stiffness
P_{v}	measured vertical stress
$P_{\text{v}}/\gamma h$	stress ratio
RC	relative compaction
R_{f}	failure ratio
r_{u}	pore water pressure ratio
UU	unconsolidated undrained
w_{opt}	optimum moisture content
α	reduction factor for ϕ
γ	unit weight
γ_{d}	dry unit weight
γ_{sat}	saturated unit weight
γ_{wet}	wet unit weight
ν	Poisson ratio
σ	stress
ϕ	internal friction angle
ψ	dilation angle

1. INTRODUCTION

A number of rockfill dams with a clay core have experienced large settlements and deformations in their upstream slopes during first impounding. Such dams include Canales,[1] Cogswell,[2] Cougar,[3] El Infiernillo,[4] Gepatsch,[5] Round Butte,[6] South Houlston,[7] El Isiro,[8] Cherry Valley,[9] LG-2,[10] and Masjed-E-Soleyman.[11] Table 1 summarises the characteristics of some rockfill dams and their behaviour during first impounding.

During first impounding of a rockfill dam with a central clay core, the effective stresses within its upstream shell are reduced owing to submerging and buoyancy effects: hence heaving and upward deformations are expected to occur in this part of the dam. However, most rockfill dams have experienced relatively large settlements in their upstream shells during first impounding. Of course, analyses encountering only reductions in effective stresses of the submerged materials will predict heaving in the upstream shell.

This paper first reviews the effects of first impounding on rockfill dams. Then it introduces the Masjed-E-Soleyman rockfill dam, Khuzestan, Iran, and reviews results of monitoring of the instruments installed in the dam. The paper introduces also numerical back-analyses of the dam for the end of construction and first impounding loading. Finally it presents the results of the analyses and compares them with the monitoring results.

2. EFFECTS OF FIRST IMPOUNDING ON ROCKFILL DAMS

First impounding has different, complicated effects on the materials and boundaries of a rockfill dam. These effects are shown schematically in Fig. 1,[12] and can be described as follows.

(*a*) E1: hydrostatic pressure acting on the core, which induces a downward, downstream-oriented movement in the dam.
(*b*) E2: hydrostatic pressure acting on the upstream foundation, which induces a downward movement and an

Dam	Height: m	Impounding duration	Max. settlement: m	Remarks	Ref.
Canales, Spain	158	NIA	0·85	Shell compacted in layers of 1·5 m	1
Infiernillo, Mexico	148	21 days	0·3	Inclined crack in core, tensile stress in left abutment	4
Cogswell, USA	85	NIA	2·6	Shell compacted dry	2
Cougar, USA	158	4 days	0·3	Some cracks in core, movement toward upstream	3
Gepatsch, Austria	120	1 month	0·5	Some longitudinal cracks in crest	5
South Holston, USA	87	4 months	0·4	8 cm horizontal movement of core centre toward upstream	7
LG-2, Canada	156	NIA	1·3—1·5	Crack in interface of core and upstream shell	10

*NIA = no information available.

Table 1. Characteristics and behaviour of rockfill dams during first impounding

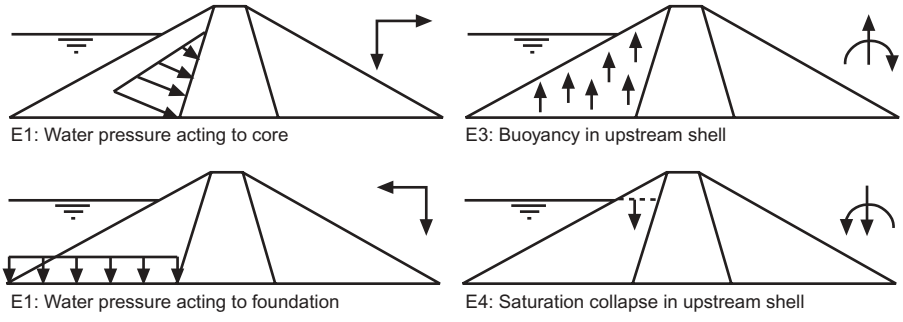

Fig. 1. Effects of impounding on rockfill dams with central clay core[12]

upstream-oriented rotation of the dam and foundation. The magnitude of E2 depends on the permeability of the foundation: the less permeable the foundation, the larger E2 during first impounding.

(*c*) E3: buoyancy effect on the upstream shell, which reduces the effective stresses in the upstream embankment, resulting in an upward movement and downstream-oriented rotation of the dam.

(*d*) E4: saturation collapse in the upstream shell, which induces a downward movement of the upstream embankment and an upstream-oriented rotation of the dam. This effect results from wetting-induced reductions of the strength and stiffness of the rockfill materials.

The last effect is relatively complicated. Whereas effects E1, E2 and E3 can be modelled readily using most geotechnical computer software, modelling of E4 is not routine, easy work, because of the complicated effects of water on the strength and stiffness properties of dry rockfills. Saturation collapse is responsible for major parts of the deformations occurring during first impounding of rockfill dams. Saturation collapse occurs only once, and its deformations are plastic and irrecoverable. A numerical analysis acceptable for modelling of first impounding loading of rockfill dams should undoubtedly take this effect into account.

Terzaghi considers major parts of the wetting-induced settlements of rocks with quartz and feldspar minerals to be the result of a reduction in strength of the rocks due to wetting,[13]. As a result of the strength reduction, angular and point contacts between rock pieces are crushed, and this in turn results in more strength reductions and settlements. The degree of the strength reduction depends on the type of rock mineral and the degree of weathering. Having appreciated the above process, Touileb *et al.* suggested that the lubrication effects of water on contact areas of rocks are also responsible for the saturation collapse.[10] The initial void ratio of the upstream rockfill is also effective in this regard.[14]

Triaxial tests on rockfill samples in dry, dry–wet, and wet conditions[7,15] have shown that wetting of dry samples during loading (so-called dry–wet tests) induces sudden settlements, as shown in Fig. 2. It can be seen that, after adding water to the sample, the stress level suddenly drops, and then the sample recovers part of its strength and stiffness.

3. MASJED-E-SOLEYMAN ROCKFILL DAM

3.1. General characteristics

The Masjed-E-Soleyman rockfill dam, with a central clay core and a maximum height of 176 m, was constructed on the Karun River, Khuzestan, Iran, from 1995 to 2000. The main purpose of the dam construction was to provide energy (1500 MW). The longitudinal section and the highest cross-section of the dam are shown in Figs 3 and 4 respectively. As shown, the upstream and downstream slopes are 2H:1V and 1·75H:1V respectively. The dam crest is 480 m long, and the coffer dam is integrated in the main dam. The dam features a relatively small-volume reservoir (228×10^6 m^3).

3.2. Dam body materials

The core materials are clayey soils with 80% fines and 20% sand and gravel, highly compacted (about 100% relative compaction) in layers of 20 cm final thickness. The average compaction moisture content was w_{opt} + 2% to provide a low-

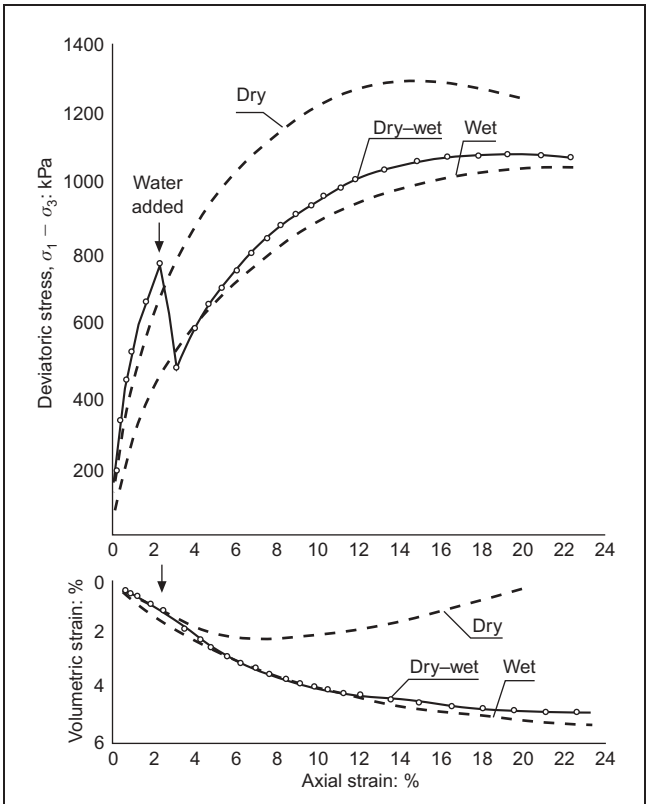

Fig. 2. Triaxial tests: dry test, wet test and dry–wet test (saturation under constant axial strain)[7]

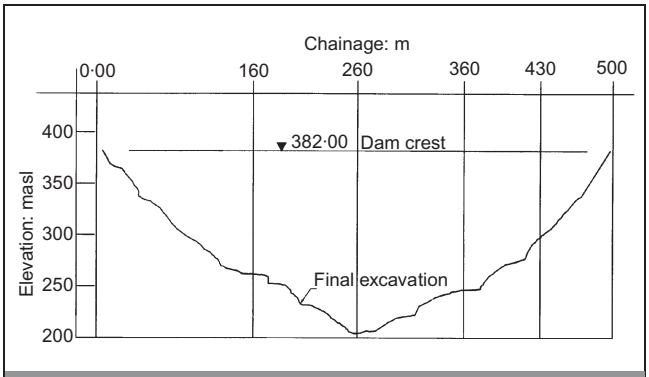

Fig. 3. Longitudinal section of Masjed-E-Soleyman dam (view from upstream)

permeability core ($k_h = 10^{-7}$ cm/s, $k_v = 10^{-8}$cm/s), and to compensate partially for evaporation. The type of compaction test was a modified effort compaction test (ASTM 1557). Quality control tests during the dam construction suggested that the average, after-compaction degree of saturation of the materials was about 95%.

The shell materials (3A, 3B, 3C, 3D) are rockfills, compacted dry in layers of about 70–100 cm final thickness. According to the quality control tests, these materials comprise approximately 4% fines, 9% sand, 27% gravel, 18% cobbles, and 42% rock pieces. It is of interest that the percentages of cobbles and rocks are relatively high. The materials are from quarries of conglomerate, sandstone and claystone, excavated from the foundation and diversion tunnels. The dam foundation comprises intercalated layers of conglomerate, claystone, sandstone and siltstone. These layers *in situ* are much stronger and stiffer than the materials of the dam.

3.3. Impounding history

The dam impounding started on 20 December 2000, one month after end of the construction. In order to have enough time for controlling safety of the structure through careful monitoring, the impounding was managed in five stages, as follows: first stage from El. 255 m to El. 280 m (25 m); second stage to El. 317 m (37 m); third stage to El. 330 m (13 m); fourth stage to El. 350 m (20 m); and fifth stage to El. 372 m (22 m). The first stage of the impounding had been achieved accidentally by a flood 10 days before the schedule. Except for the fifth stage, the impounding rate was relatively high and a challenge for the project, owing to the relatively small volume of the reservoir and a lack of sufficient control on the river flow. The fifth stage of impounding was not achieved according to the schedule; it was delayed by some unforeseen technical problems.

3.4. Instrumentation results

Four sections of the dam, CH160, CH260, CH360 and CH435 as shown in Fig. 3, were instrumented with pressure cells, piezometers, surface settlement marks, settlement gauges and inclinometers. A considerable number of the instruments, especially in the upstream slope, were subjected to damage, and therefore malfunctioned during the impounding. A typical instrumented cross-section for CH260 is presented in Fig. 4. Typical results of monitoring of the un-damaged instruments are presented below.

Deformations. Figure 5 shows the settlement history for a number of points within the core for CH260. These settlements occurred during construction of about the last 75 m height of the dam and impounding up to El. 372 m. Fig. 6 presents the history of surface settlements taken from the bench marks for different points of the core and upstream shell, compared with variations of the reservoir level up to El. 338 m. During this period, a maximum settlement of about 7 cm occurred in the downstream shell. As the benchmarks were installed on 15 January 2001, surface settlements for the first 25 days of the impounding were missed. Moreover, no information about surface settlements before impounding was available. Fig. 7 shows horizontal displacements, in the direction of the dam axis, of a number of points for six cross-sections of the dam; these displacements were measured from movements of the surface bench marks five months after the impounding.

Total stresses and pore water pressures. Figure 8 presents variations of normalised total vertical stresses for a number of points in the core along with reservoir level variations during the first month of impounding. The stresses are normalised to total vertical stresses before impounding. Table 2 shows total vertical stress ratios, $P_v/\gamma h$ (where P_v is measured total vertical stress), for a number of points within the core, downstream filters and downstream shell:

(*a*) immediately before impounding
(*b*) two months after impounding
(*c*) five months after impounding
(*d*) the difference between (*c*) and (*a*).

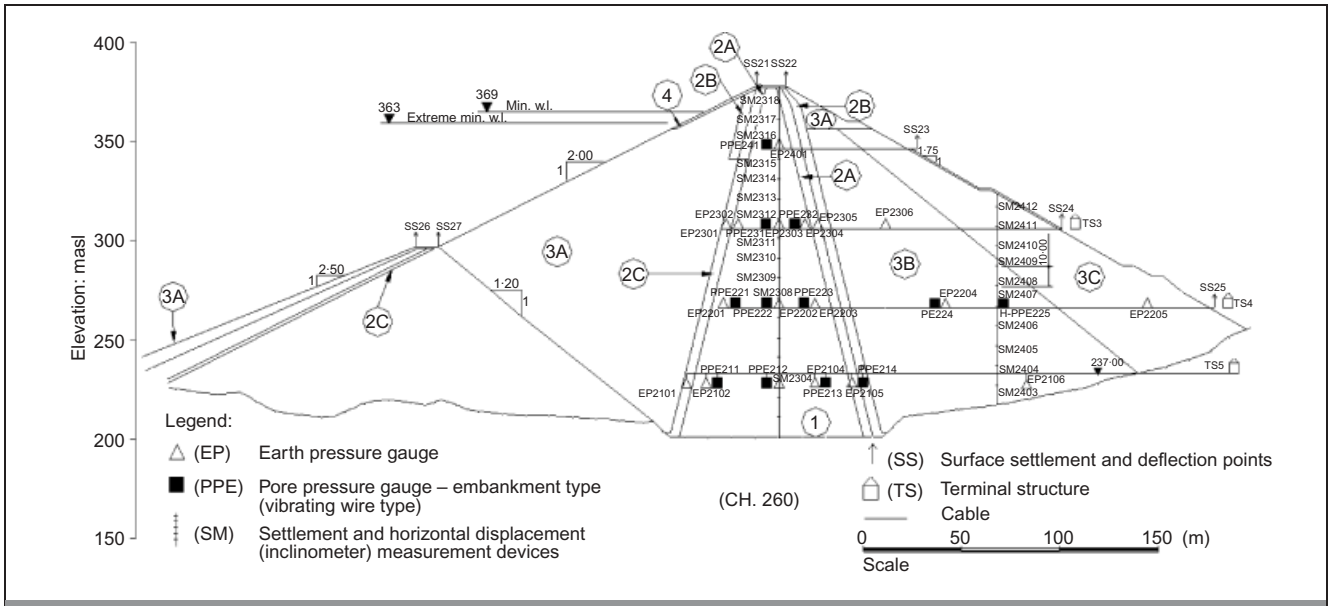

Fig. 4. Instrumented cross-section of Masjed-E-Soleyman dam (CH260)

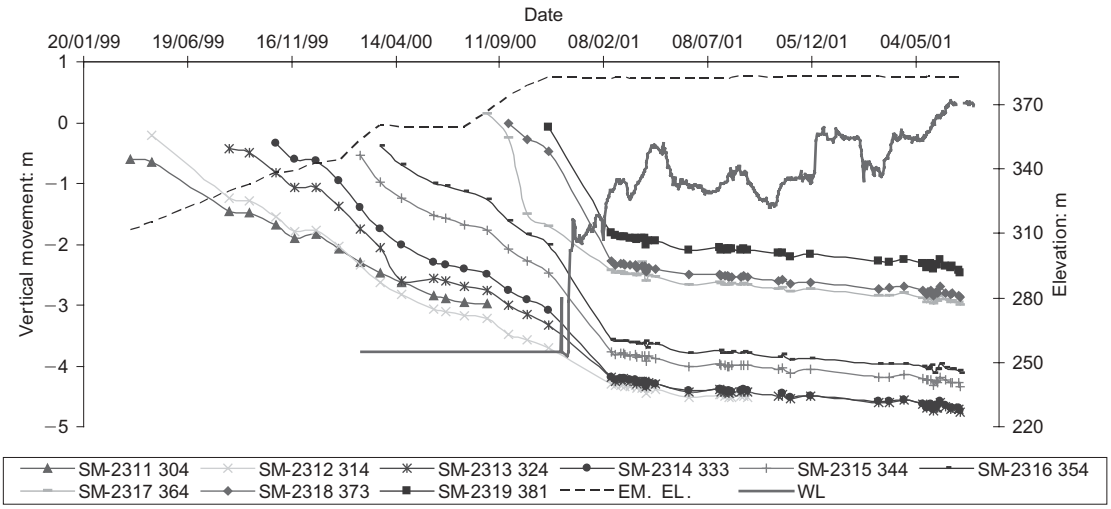

Fig. 5. Settlement history within the core for CH260

Table 3 shows pore water pressure ratios, r_u (the ratio of measured pore water pressure to γh) in the centre and downstream of the core:

(*a*) before impounding
(*b*) five months after impounding
(*c*) nine months after impounding
(*d*) the difference between (*b*) and (*a*).

3.5. Evaluation of instrumentation results and dam behaviour

3.5.1. Evaluation of instrumentation results

Deformations. Figure 5 shows that the core has evidently settled mostly during the dam construction, with a maximum value of about 3·6 m for El. 314 m. The impounding-induced settlements of the core have resulted mostly from lateral bulging and not from consolidation. This idea is supported by the history of pore water pressures (Table 3), which indicates a relatively low permeability for the core and practically no consolidation occurring during the impounding. Fig. 6 shows that from 15 January to 10 April, with 26 m (312 to 338 m) rising of the reservoir elevation, maximum settlements of about 27 cm and 20 cm occurred respectively in the core (CH260) and upstream shell (El. 360 m, CH260). In general, the core settled more than the upstream shell, and the upstream shell settled more than the downstream shell. Fig. 7 indicates that the dam sections moved generally towards the valley centre: that is, CH80, CH160 and CH260 toward the right abutment and CH360, CH420 and CH470 toward the left abutment (view from upstream).

Total stresses and pore water pressures. Figure 8 suggests that, for all the pressure cells within the core, the total stresses have increased as a result of raising the reservoir level to El. 317 m. This indicates that the net result of reservoir impounding is a

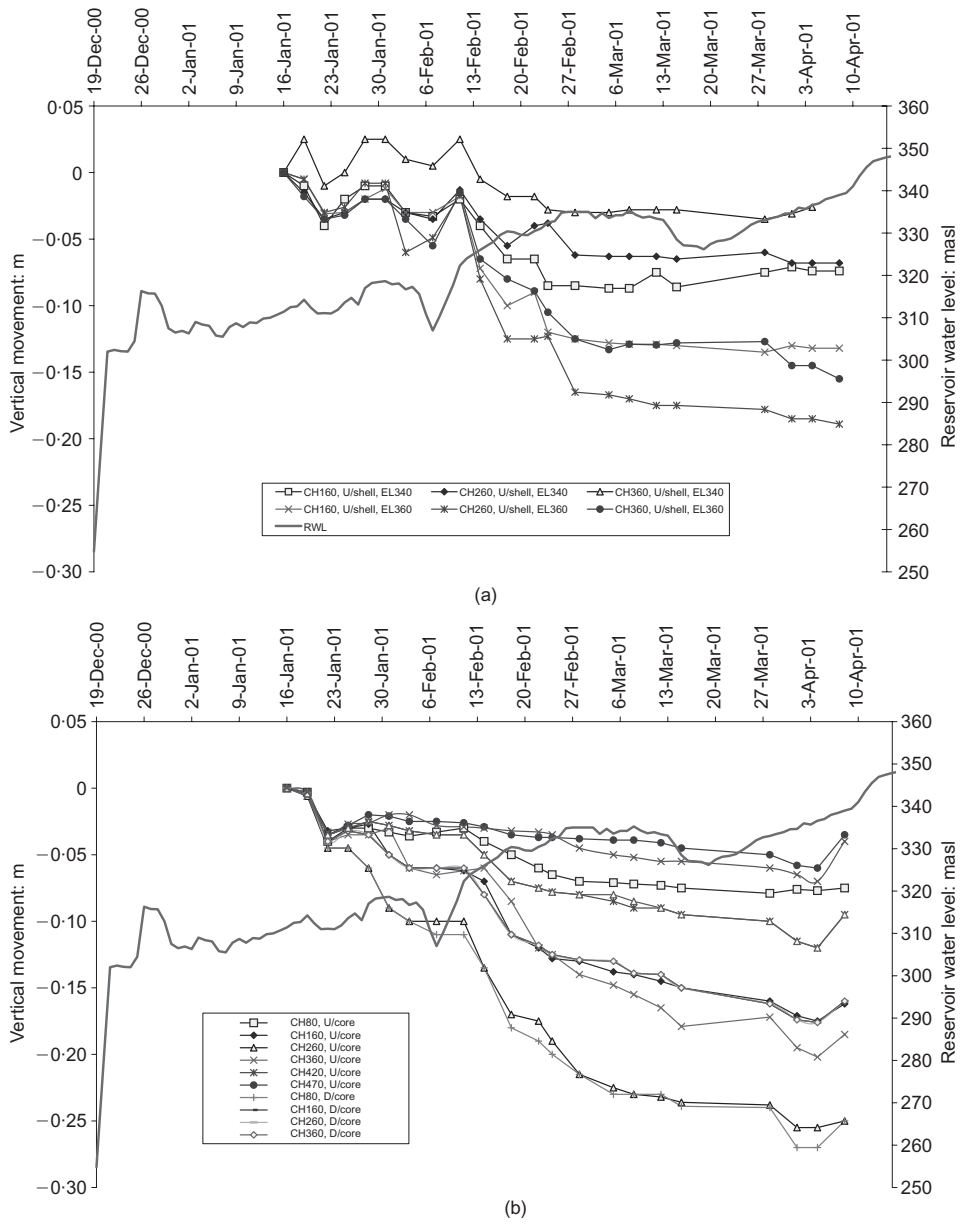

Fig. 6. History of surface settlements with respect to reservoir elevation: (a) upstream shell; (b) core crest (upstream/downstream)

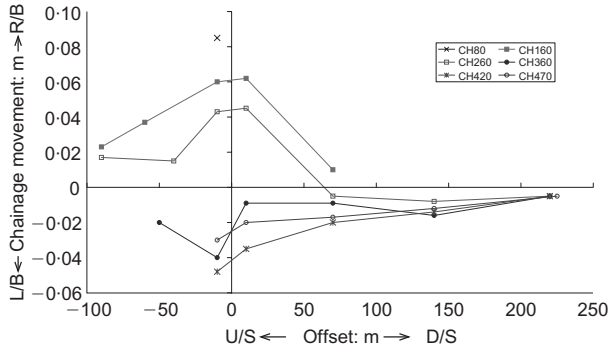

Fig. 7. Impounding-induced horizontal surface displacements in dam axis direction for different dam cross-sections

loading effect on the core, and that the combination of effects E1, E2 and E4 overcomes the effect of E3 (see Fig. 1).

Table 2 clearly shows arching phenomena at the end of construction: that is, a minimum value of stress ratio ($P_v/\gamma h$) of 0·46 in the core (El. 310 m, CH260), a maximum value of 1·75 in the filter (El. 310 m, CH360), and intermediate values for the shells. Table 2 also shows that, after the impounding, the stress ratios in the core have generally increased, and those in the downstream filters and shell have decreased (compare columns 'd' for the core, filter and shell.). This stress redistribution was induced by the combined loading effects of E1, E2 and E4 on the core.

Table 3 shows that in general the values of r_u have increased as a result of impounding, with a maximum r_u of 0·73 at El. 230 m, CH260, and a maximum increase of r_u of 0·08 at El.

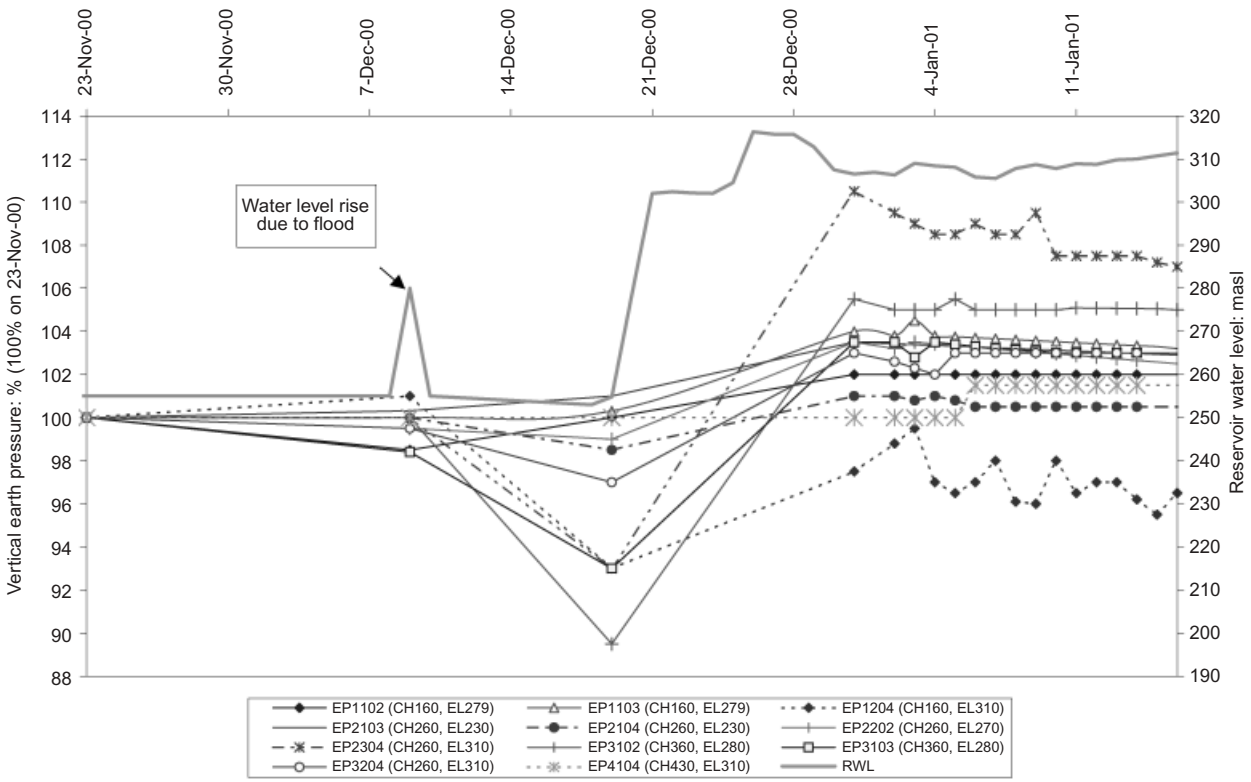

Fig. 8. History of normalised total vertical stresses in core with respect to reservoir elevation

CH: m	El: m above sea level	Stress ratio, $P_v/\gamma h$														
		Core (centre line)				Core (downstream)				Filter (downstream)				Shell (3B)		
		a	b	c	d	a	b	c	d	a	b	c	d	a	c	d
160	280	0·67	0·69	0·71	0·04	0·66	0·64	0·72	0·06	–	–	–	–	–	–	–
160	310	–		–	–	0·59	0·58	0·61	0·02	1·45	1·43	1·39	−0·06	1·14	1·09	−0·05
260	230	0·68	0·7	0·71	0·03	0·78	0·77	0·79	0·01	1·4	1·4	1·34	−0·06	0·56	0·51	−0·06
260	270	0·6	0·62	0·66	0·06	0·65	0·67	0·69	0·03	–	–	–	–	–	–	–
260	310	–		–	–	0·46	0·48	0·53	0·07	1·64	1·64	1·59	−0·05	0·84	0·78	−0·06
360	280	0·65	0·71	0·65	0	0·66	0·7	0·69	0·03	–	–	–	–	1·08	1·1	0·02
360	310	–		–	–	0·6	0·6	0·65	0·05	1·75		1·76	0·01	0·65	0·58	−0·07
430	310	–		–	–	0·62	0·61	0·64	0·02	1·3		1·27	−0·03	1·06	0·9	−0·16

Key: (a) immediately before impounding; (b) two months after impounding; (c) five months after impounding; (d) difference between (c) and (a).

Table 2. Total vertical stress ratio in the core, downstream filter and shell

310 m, CH260, both in the downstream core. It is also evident that the values of r_u 9 months after impounding (case c) decreased and approached the values before impounding values. It is evident that the piezometer responses are consistent with the pressure cell responses in the core. Undrained loading, which is induced by the hydrostatic pressure on the upstream slope of the core (E1) and the saturation settlement of the upstream shell (E4), has generated pore water pressure. The behaviour of the piezometers in the core during impounding suggests again that the combination of effects E1 and E4 overcame the effect of E3.

3.5.2. Evaluation of dam behaviour during impounding. The evaluation of the instrumentation results leads us to the following conclusion regarding the dam behaviour, especially collapse compression in the upstream rockfill, during the first impounding.

The only systematic measurement of collapse compression in the upstream rockfill is that shown in Fig. 6, which shows a maximum compression of about 20 cm (El. 360 m, CH260) for only 26 m of the rise of the reservoir. Further random geodetic surveys performed on a few bench marks located in the higher elevations of the upstream rockfill showed that about 180 cm maximum settlement occurred (CH260) at the end of the fourth stage of impounding.

Figure 5 indicates that the maximum vertical downward

CH: m	El.: m above sea level	(a)		(b)		(c)		(d)	
		Core (C/L)	Core (D/S)	Core (C/L)	Core (D/S)	Core (C/L)	Core (D/S)	Core (C/L)	Core (D/S)
160	280	0·61	0·62	0·64	0·67	0·61	0·63	+0·03	+0·04
160	310	–	0·36	–	0·43	–	0·4	–	+0·07
260	230	0·65	0·7	0·68	0·73	0·67	0·7	+0·02	+0·03
260	270	0·59	0·63	0·63	0·68	0·6	0·63	+0·04	+0·05
260	310	–	0·32	–	0·4	–	0·37	–	+0·08
360	280	0·56	0·59	0·61	0·63	0·59	0·59	+0·04	+0·04
360	310	–	0·41	–	0·47	–	0·45	–	+0·06
430	310	–	0·34	–	0·36	–	0·33	–	+0·02

Key: (a) immediately before impounding; (b) 5 months after impounding; (c) 9 months after impounding; (d) difference between (b) and (a); C/L, centre line; D/S, down stream.

Table 3. Pore water pressure ratios, r_u, in centre and downstream of core

movement of the core during the full impounding of the reservoir has been about 180 cm; this movement for the end of the fourth stage of impounding has been about 150 cm. As the permeability of the core was very low, and pore water pressures have been either constant or increasing during the impounding (Table 3), we believe that vertical deformations of the core during impounding have not been due to consolidation; rather they have been caused by lateral bulging of the core, induced by compression of the upstream shell.

Some observations showed longitudinal cracks in the dam crest and separations between the shell and core in the upstream filter area, indicating larger settlements in the upstream shell than in the core.

Considering the above, we may conclude that an approximate maximum collapse compression in the range 180–200 cm has occurred in the upstream rockfill. As the upstream shell was compacted dry, and precipitation was rare during the last two years of dam construction, saturation collapse settlements were expected during the first impounding. This phenomenon reduced arching effects, increased pore water pressures, and induced downward movements in the core.

3.6. Numerical analysis

3.6.1. Analysis procedure. We carried out numerical back-analyses of dam cross-sections CH160, CH260, CH360 and CH435 after the fourth stage of impounding had been completed (reservoir El. 350 m). For each of the sections we modelled the dam height in 10 m layers. Effective strength parameters for the shell and filter materials and total strength parameters for the core material were introduced into the analyses. Numerical analyses of CH260 showed that the foundation does not affect stresses and strains within the dam body, as it is comparatively much stronger and stiffer than the dam. Therefore we excluded the foundation from the modelling of the other cross-sections.

The loading during construction was analysed by simulating the stages involved in the dam construction. The impounding loading was modelled according to the impounding history by

(*a*) applying hydrostatic boundary pressures on the upstream slope of the core (E1)
(*b*) applying hydrostatic boundary pressures on the upstream foundation (E2)
(*c*) reducing the unit weights of the upstream shell materials to their submerged values (E3)
(*d*) reducing the strength parameters and deformation moduli of the upstream shell materials, in order to account for saturation and submergence effects (E4).

3.6.2. Material properties. Representative material properties and input parameters for the analyses were based on laboratory, field and quality control tests. Table 4 summarises the properties of the core material. Results from the large-scale triaxial tests conducted on the shell materials (800 mm × 800 mm for 3A and 200 mm × 420 mm for 3B) indicated that the internal friction angles of these materials decrease with increasing effective vertical stress, according to the following equation:

$$\phi = \phi_{\max} - \alpha \log\left(\frac{\sigma_n}{\sigma_0}\right) \quad (1)$$

where σ_n is the effective vertical stress at an arbitrary depth, σ_0 is the effective vertical stress at a depth of 10 m, ϕ is the internal friction angle associated with σ_n, $\phi_{\max}$ is the maximum internal friction angle, associated with σ_0, and α is a reduction factor.

An average friction angle for the materials of each of the rockfill zones was calculated. Table 5 summarises the properties of the shell and filter materials.

MC	w_{opt}	γ_d: kN/m^3	γ_{wet}: kN/m^3	RC	PI	c: kN/m^2	ϕ: deg	Test type
15·2	13·8	18·2	21·0	100	18·7	85	3·7	UU (saturated)

Table 4. Material properties of core from laboratory and quality control tests

Material	γ_d: kN/m^3	γ_{sat}: kN/m^3	γ_{wet}: kN/m^3	RC	ϕ_{max}, dry: deg	ϕ_{avg}: deg	
						Dry	Saturated
2A	19·2	21·7	20·4	90	39	35	33
2B	17·7	20·5	18·1	92	48	41	39
2C	21·1	23·5	22·6	100	–	41	39
3A	22·2	23·9	22·8	90	56	45	41
3C	23·3	24·6	23·5	91	56	45	41
3B	23·0	24·0	23·4	88	46	41	41

Table 5. Material properties of shell and filters from laboratory and quality control tests

3.6.3. Behaviour model. The elasto-plastic Hardening Soil model,[16] adopted in the PLAXIS finite element computer code,[17] was employed for the numerical analyses. This model uses principles of the hyperbolic model,[18] and formulates plastic stresses and strains. The Hardening Soil model supersedes the hyperbolic model by:

(*a*) using the theory of plasticity rather than the theory of elasticity
(*b*) including soil dilatancy
(*c*) introducing a yield cap.

The model computes volume changes induced by dilation, and employs the yield cap for defining volumetric failures. Some basic characteristics of the model are as follows:

(*a*) stress-dependent stiffness according to a power law (input parameter m)
(*b*) plastic straining due to primary deviatoric loading (input parameter E_{50}^{ref})
(*c*) plastic straining due to primary compression (input parameter E_{oed}^{ref})
(*d*) elastic unloading/reloading (input parameters E_{ur}^{ref}, ν_{ur})
(*e*) failure according to the Mohr–Coulomb model (input parameters c, ϕ and ψ).

In order to verify the hardening soil model, and also to estimate the special parameters for the model, we simulated numerically the triaxial tests that had been performed on the materials of the different zones of the dam during the design phase of the project. For example, Fig. 9 compares the results of the verification analyses with the results of the large-scale triaxial tests on material 3A. Similar favourable results were obtained for the other materials of the dam. This type of verification and modelling suggested that the Hardening Soil model enables us to simulate the behaviours of the materials. Table 6 presents the mechanical parameters used in the numerical analyses for the end of construction and the first impounding loading.

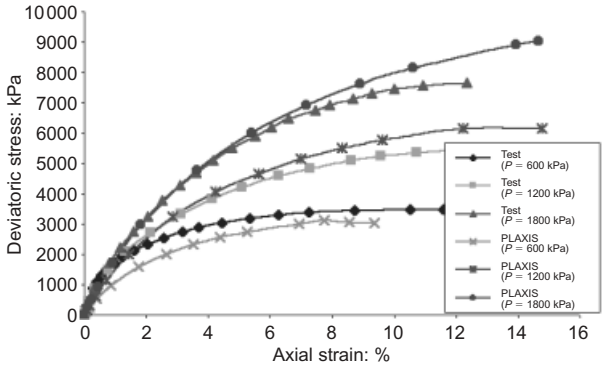

Fig. 9. Computed and test results of triaxial testing on material 3A

In order to encounter the effect of impounding-induced wetting (i.e. dry–wet conditions) on the degradations of strength and deformation parameters of the upstream shell materials (see Fig. 2), the internal friction angle and stiffness values were reduced, as shown in Table 6. This was based on a number of back-analyses and a consideration of published work on this subject. For numerical modelling of wetting-induced settlements of the LG-2 Dam, Quebec, Canada, ϕ of the upstream material was reduced from 45° to 40°.[10] Other researchers have reduced the internal friction angles and stiffness of rockfill materials when they are rapidly saturated.[19,20] The level of the reduction depends on various

Material	Test condition	c: kN/m^2	ϕ: deg	$E_{50}^{ref} \times 10^3$: kN/m^2	$E_{oed}^{ref} \times 10^3$: kN/m^2	$E_{ur}^{ref} \times 10^3$: kN/m^2	m	P_{ref}: kN/m^2	R_f	ν	ψ: deg
2A	Dry	0	35	72	107	198	0·50	1200	0·8	0·36	5
2B	Dry	0	41	72	107	198	0·50	1200	0·8	0·33	11
2C	Dry	0	41	126	185	378	0·50	1200	0·8	0·30	11
3A, 3C	Dry	0	45	117	118	378	0·35	1200	0·8	0·30	15
3B	Dry	0	41	117	118	378	0·35	300	0·8	0·30	11
3A	Dry–wet	0	30	50	50	100	0·50	1200	0·8	0·30	0
2C	Dry–wet	0	30	55	55	110	0·50	1200	0·8	0·30	0
Core	Wet	85	3·7	18	36·6	54	0·90	600	0·9	0·45	0

Table 6. Strength and deformation parameters used in elasto-plastic analyses

parameters and factors, including the type, weathering degree, and size of the rockfills. As the stiffness is stress dependent in the Hardening Soil model, the stiffness of the upstream shell materials was reduced owing to submergence effects. Note that no data about the mechanical properties of the shell materials of the dam in 'dry–wet' conditions were available, because no tests in such conditions had been carried out.

3.6.4. Results of numerical analyses and comparison with results of instrumentation. Extensive results from numerical analyses of the four dam cross-sections were provided. Some typical results are selected and compared with the monitoring results. The fact that the dam is built in a steep-sided valley, and the analyses assumed plane strain conditions, may be responsible for some discrepancies between the measured and computed results.

Before impounding. Figure 10 presents the distribution of the computed mean normal total stresses at El. 310 m, CH260 of the dam; the arching effect (i.e. low stresses in the core and high stresses in the filters and shells) is evident. Fig. 11 shows the computed shear stresses at the same elevation: as expected, the shear stress in the core centreline is a minimum (zero), and in the filters and transition zones is a maximum.

Figure 12(a) presents computed and measured total vertical stresses for three points in the downstream embankment at El. 310 m, CH160. The measured and computed stresses compare favourably for the core and filters; in the shell, however, the computed stresses are considerably larger than the measured stresses. It can be seen that the stresses in the core and in the filter are a minimum and maximum respectively, which again represents the arching effect. Fig. 12(b) presents computed and measured total vertical stresses for four points in the downstream embankment at El. 230 m, CH260. Relatively good agreement between the computed and measured results can be observed, especially in the core and filter. Fig. 13(a) and 13(b) compare the computed and measured absolute settlements along the dam height on the core centreline for CH260 and CH360 respectively during the dam construction. There is

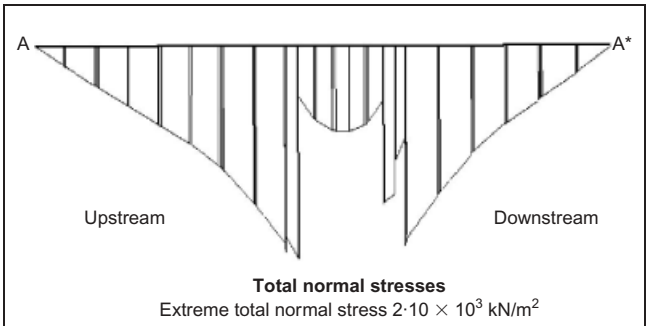

Fig. 10. Distribution of computed mean normal total stresses at El. 310 m, CH260 (end of construction)

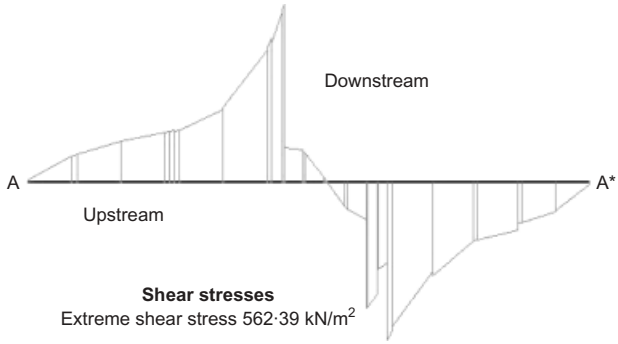

Fig. 11. Distribution of computed shear stresses at El. 310 m, CH260 (end of construction)

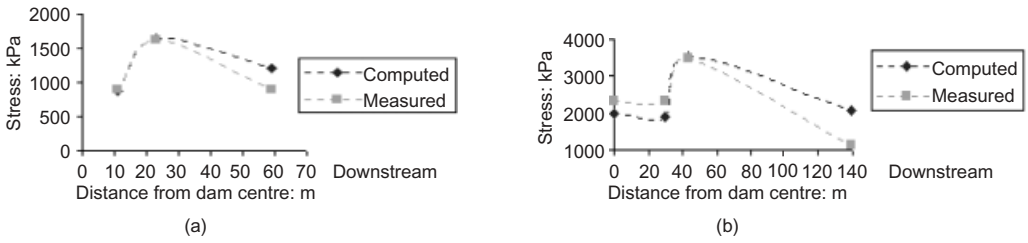

Fig. 12. Computed and measured total vertical stresses (end of construction): (a) El. 310 m, CH160; (b) El. 230 m, CH260

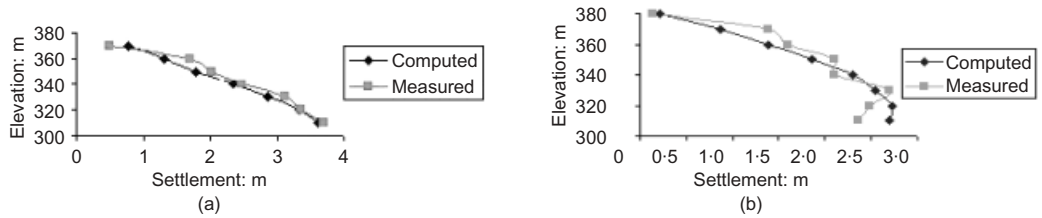

Fig. 13. Computed and measured absolute settlements along dam height in core centreline (end of construction): (a) CH260; (b) CH360

reasonable agreement between the computed and measured settlements.

After impounding (reservoir El. 350 m). Figure 14 presents the distribution of computed mean normal total stresses at El. 310 m, CH260 of the dam; for the upstream shell, the effective stresses are also shown. By comparing this figure with Fig. 10, we find that arching is reduced on the upstream side of the core after impounding. The hydrostatic boundary pressure on the upstream slope of the core and saturation collapse settlements of the upstream shell are jointly responsible for this reduction. Fig. 15 presents computed horizontal displacements

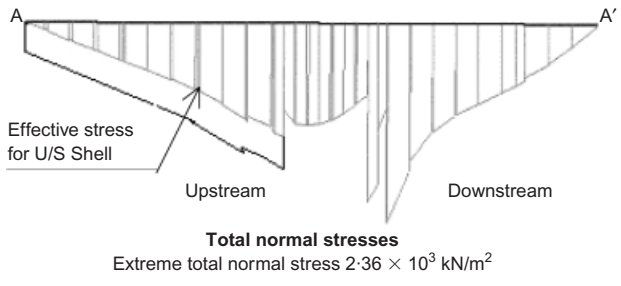

Fig. 14. Distribution of computed mean normal total stresses at El. 310 m, CH260 (reservoir El. 350 m)

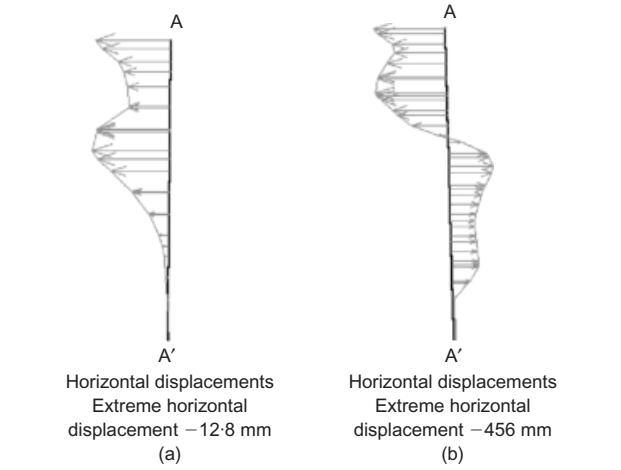

Fig. 15. Computed horizontal displacements on dam centreline for CH260: (a) before impounding; (b) after impounding (reservoir El. 350 m)

of the dam centreline for CH260 before and after impounding. Fig. 15(a) indicates that the end-of-construction horizontal displacements, with a maximum value of 12·8 mm, are in the upstream direction, probably as a result of asymmetry of the cross-section. Fig. 15(b) shows that the upper elevations moved toward the upstream, with a maximum value of 456 mm, and the lower elevations moved toward the downstream.

Figure 16(a) and 16(b) present computed and measured total vertical stresses for three points in the downstream slope at El. 310 m for CH260 and CH360 respectively. Generally, there is reasonable agreements between the computed and measured stresses. The comparatively lower measured values may indicate across-valley arching effects. Figure 17(a) and 17(b) present computed and measured absolute settlements along the dam height on the core centreline for CH160 and CH260 respectively, for the period between dam construction and impounding up to El. 350 m. For CH260, which is near the deep valley section, and therefore less influenced by 3D effects, there is better agreement between the computed and measured values.

4. SUMMARY AND CONCLUSIONS

This paper has reviewed the effects of first impounding on rockfill dams. Among these effects, the saturation collapse phenomenon was dealt with in more detail. Special attention was paid to the effects of saturation on the mechanical behaviour of dry-placed rockfills. A comprehensive study of the behaviour of the Masjed-E-Soleyman rockfill dam during its construction and first impounding has been presented. The study has included analyses of the instrumentation results and finite element back-analyses.

The results of the instrumentation showed that impounding-induced saturation compressions occurred in the upstream rockfill, which had been compacted dry during construction. This phenomenon reduced arching, increased pore water pressures, and induced settlements in the dam core. During the first impounding of the Masjed-E-Soleyman rockfill dam, the loading effect of saturation collapse overcame the unloading effect of submergence of the upstream shell.

The numerical analyses of the dam have indicated that the hardening soil model, using reduced strength and stiffness parameters for rockfills in the dry–wet condition, enables one to capture the behaviour of the dam during first impounding. The results of the analysis, in terms of stresses and deformations, compared well with the results of the instrumentation monitoring.

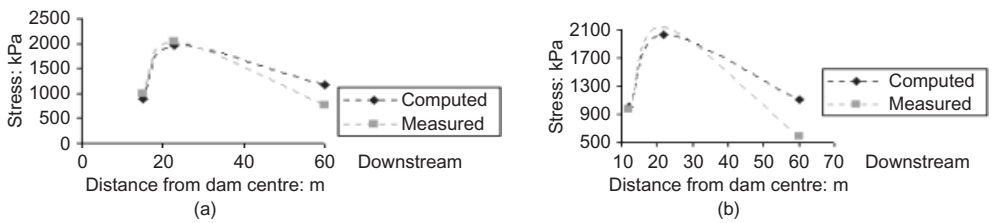

Fig. 16. Computed and measured total vertical stresses in core, filter and downstream shell for reservoir level at El. 350 m: (a) El. 310 m, CH260; (b) El. 310 m, CH360

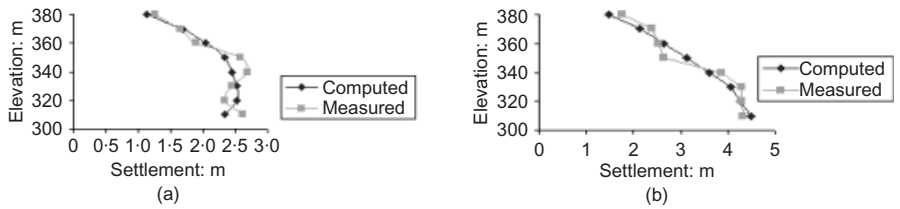

Fig. 17. Computed and measured settlements for different elevations of core centreline for reservoir level at El. 350 m: (a) CH160; (b) CH260

5. ACKNOWLEDGEMENTS

Financial support and data provided by the Masjed-E-Soleyman Project, Iran Water and Power Resources Development Company (IWPC), as the project client, are acknowledged. The authors are also thankful to the client for permitting them to publish the field data.

REFERENCES

1. POSSE J. A., HERMOSILLA R. P. and SANTAMARIA J. M. M. Monitoring of the Canales dam and its control during construction period. *Proceedings of 2nd International Conference on Case Histories in Geotechnical Engineering*, St Louis, MO, 1988, 677–682.
2. BAUMANN P. Cogswell and San Gabriel dams. *Transactions ASCE*, 1960, **125**, No. 2A, 29–57.
3. POPE R. J. Evaluation of Cougar dam embankment performance. *Journal of the Soil Mechanics and Foundation Division, ASCE*, 1967, **93**, No. 4, 261–264.
4. MARSAL R. J. and DE ARELLANO L. R. Performance of El Infiernillo dam, 1963–1966. *Journal of the Soil Mechanics and Foundation Division, ASCE*, 1967, **93**, No. 4, 265–298.
5. SCHOBER W. Behavior of Gepatsch rockfill dam. *Proceedings of the 9th International Congress on Large Dams*, Istanbul, 1967, **3**, 677–699.
6. PATRICK J. G. Post construction behavior of Round Butte dam. *Journal of the Soil Mechanics and Foundation Division, ASCE*, **93**, No. 4, 251–260.
7. NOBARI E. S. and DUNCAN J. M. *Effect of Reservoir Filling on Stresses and Movements in Earth and Rockfill Dam.* University of California, Berkeley, 1972, Geotechnical Engineering Report No. TE-72-1.
8. SHERARD J. L. Embankment dam cracking. In *Embankment-Dam Engineering* (HIRSCHFELD R. C. and POULOS S. J. (eds)), Wiley, New York, 1973, pp. 271–351.
9. HAYASHI M. Progressive submerging settlement during water loading to rockfill dam: initial strain analysis, material property and observed result. *Proceedings of an International Symposium*, Swansea, 1975, pp. 868–880.
10. TOUILEB B. N., BONELLI S., ANTHINIAC P., CARRERE A., DEBORDES O., LA BERBERA G., BANI A. and MAZZA G. Settlement by wetting of the upstream rockfills of large dams. *Proceedings of the 53rd Canadian Geotechnical Conference, Montreal*, 2000, **1**, 263–270.
11. AGHAEI ARAEI A. *Back Analysis of Deformations Induced During First Impounding of the Masjed-E-Soleyman Rockfill Dam*. MSc thesis, Amirkabir University of Technology, Tehran, Iran, 2002.
12. INTERNATIONAL COMMISSION ON LARGE DAMS. *Static Analysis of Embankment Dams*. ICOLD, Paris, 1986, Bulletin No. 53.
13. TERZAGHI K. Discussion on Salt Spring and Lower Bear River. *Transactions of American Society of Civil Engineers*, 1960, **125**, Part 2, 139–148.
14. MORI Y., SHIMOKAWA H. and NAKANO Y. Analysis of zoned rockfill dam with center core during construction and first filling. *Proceedings of the 20th Congress on Large Dams, Beijing*. ICOLD, Paris, 2000, Vol. II, pp. 1309–1336.
15. BONELLI S. and ANTHINIAC P. Modelisation hydroplastique du premier pemplissage d'un barragien enrochemen. *Proceedings of the 53rdCanadian Geotechnical Conference, Montreal, 2000,* **1**, *252–262*.
16. SCHANZ T., VERMEER P. A. and BONNIER P. G. The Hardening Soil model—formulation and verification. In *Beyond 2000 in Computational Geotechnics: Ten Years of Plaxis International* (BRINKGREVE R. B. J. (ed.)). Balkema, Amsterdam, 1999, pp. 281–296.
17. BRINKGREVE R. B. J. and VERMEER P. A. *PLAXIS Finite Element Code for Soil and Rock Analyses, Version 7*. Plaxis BV, Delft, 1998.
18. DUNCAN J. M. and CHANG C.-Y. Nonlinear analysis of stress and strain in soils. *Journal of the Soil Mechanics and Foundation Division, ASCE*, 1970, **96**, No. SM5.
19. SOBOYA J. R. F. and BYRNE P. M. Parameters for stress and deformation analysis of rockfill dams. *Canadian Geotechnical Journal*, 1993, **30**, No. 4, 690–701.
20. VARADARAJAN A., SHARMA K. G., VENKATACHALAM K. and GUPTA A. K. Testing and modeling two rockfill materials. *Journal of Geotechnical and Geoenvironmental Engineering, ASCE*, 2003, **129**, No. 3, 206–217.